



## Tannin-grafted aminated silicon adsorbents: adsorption performance of rare earth ions coexistence

Rui-lin Yang<sup>a</sup>, Ya-chun Liu<sup>a</sup>, Qian Liu<sup>a</sup>, Tian-tian Xu<sup>a</sup>, Ke Zhu<sup>a</sup>, Yue-yue Shen<sup>a</sup>,  
Yang Liao<sup>a,b,\*</sup>, Shi-lin Zhao<sup>a,b,\*</sup>

<sup>a</sup>College of Chemistry and Materials Science, Sichuan Normal University, Chengdu, Sichuan 610068, China, emails: 1484682653@qq.com (R.-l. Yang), 549742771@qq.com (Y.-c. Liu), 350466906@qq.com (Q. Liu), 1084927895@qq.com (T.-t. Xu), 841052705@qq.com (K. Zhu), shen028@163.com (Y.-y. Shen), Tel./Fax: +86 02884761393; emails: 153796826@qq.com (Y. Liao), zhaoslin@aliyun.com (S.-l. Zhao)

<sup>b</sup>The Engineering Center for the Development of Farmland Ecosystem Service Function, Sichuan Normal University, Chengdu, Sichuan 610068, China

Received 13 December 2015; Accepted 17 March 2016

### ABSTRACT

Rare earth ions (REIs) are playing very important roles in modern industries. However, the huge amount of smelting water containing various types of REIs was difficult to separate, which often lead to difficulty in recovery of REIs and water pollution in environment. Selective adsorption was an effective route to recover the REIs in smelting water. Two adsorbents (SiO<sub>2</sub>-BT, SiO<sub>2</sub>-BWT) were prepared by grafting plant tannins (Bayberry tannin, Black wattle tannin) onto aminated silica. The as-prepared adsorbents have exhibited a high adsorption capacity to four typical REIs and high selectivity to La<sup>3+</sup> among these four REIs (La<sup>3+</sup>, Ce<sup>3+</sup>, Pr<sup>3+</sup>, Nd<sup>3+</sup>). Furthermore, the after-used adsorbents can be easily regenerated by 0.1 mol/L HNO<sub>3</sub> solution indicating superior reusability.

*Keywords:* Rare earth ions; Selective adsorption; Coexistence

### 1. Introduction

Rare earth elements (REE) are widely used in the field of chemical engineering, metallurgy, nuclear energy, optical, and luminescence because of their unique chemical and physical properties. Because of the ongoing development of modern industry, there is an ever-increasing demand for REE [1]. However, during the productive process of REE, huge amount of smelting water containing various types of rare earth ions (REIs) was generated [2,3].

There is a continuous need for new separation techniques, by which REIs can be selectively extracted and recovered from smelting water. Many separation methods such as precipitation [4], chemical reduction, ion exchange [5,6], membrane separation [7], adsorption [8,9], and biological treatment have been used to recover REIs from smelting water [10–12]. Among these methods, adsorption is an effective and simple method in treating smelting water containing various types of REIs and many effective kinds of adsorbents were synthesized. However, separating the target light REE from each other efficiently is still a challenge for their similar properties. Recovery of REIs using biosorbents, such as algae [13,14], bacteria [15], Platanus

\*Corresponding authors.

orientalis leaf powder [16], activated carbon from rice husks [17–19], and bamboo charcoal [20] are attractive for their environmental-friendly properties and high efficiency.

Plant tannin is a kind of natural polyphenol which widely exists in roots, barks, leaves, and fruits of plants. There are plenty of hydroxyls on the benzene ring backbones of tannins, which show high affinity to various types of metal ions [21]. Tannin-modified adsorbents showed high efficiency in selective recovery of transition metal ions ( $\text{Cr}^{3+}$ ,  $\text{Cu}^{2+}$ ) and actinide elements (uranium ions) [22–24]. Therefore, tannin may also exhibit excellent performance in the recovery of REIs. However, plant tannin is water-soluble which couldn't be used as adsorbent directly. Thus, aminated modified silica ( $\text{SiO}_2\text{-NH}_2$ ) is often used as a support matrix for immobilization of plant tannins because of its porous structure and physical–chemical stability. In our previous study, aminated modified silica modified by typical tannins, bayberry tannins (BT), and black wattle tannins (BWT) (Fig. 1), has exhibited high efficiency in the recovery of  $\text{Pr}^{3+}$  and  $\text{Nd}^{3+}$  in water [25]. As a continuation study, the as-prepared adsorbents are utilized in selective recovery of the other

typical light REIs ( $\text{La}^{3+}$ ,  $\text{Ce}^{3+}$ ,  $\text{Pr}^{3+}$ ,  $\text{Nd}^{3+}$ ) from simulated real smelting water.

## 2. Experimental sections

### 2.1. Reagents and characterizations

$\text{CeO}_2$ ,  $\text{La}_2\text{O}_3$ ,  $\text{Pr}_2\text{O}_3$ ,  $\text{Nd}_2\text{O}_3$ , and other reagents were of analytical grade, which were purchased from Kelong chemical reagents factory (Chengdu, China). Deionized water was used for the preparation of all solutions. The REIs solution simulated real smelting water which contained  $\text{La}^{3+}$  (14.40 mmol/L, 36.5 wt.%),  $\text{Ce}^{3+}$  (17.84 mmol/L, 47.9 wt.%),  $\text{Pr}^{3+}$  (1.77 mmol/L, 4.1 wt.%) and  $\text{Nd}^{3+}$  (3.47 mmol/L, 10.0 wt.%), respectively.

The BT and BWT were extracted from the barks of bayberry trees and black wattle trees.

The concentrations of REIs in the solution were determined by an Inductively Coupled Plasma Optical Emission Spectrometer (ICP-OES, Optima, 8000DV, Perkin-Elmer, US). The morphology of the adsorbents was observed with scanning electron microscope (SEM, FEI Quanta 250). The adsorbents were charac-

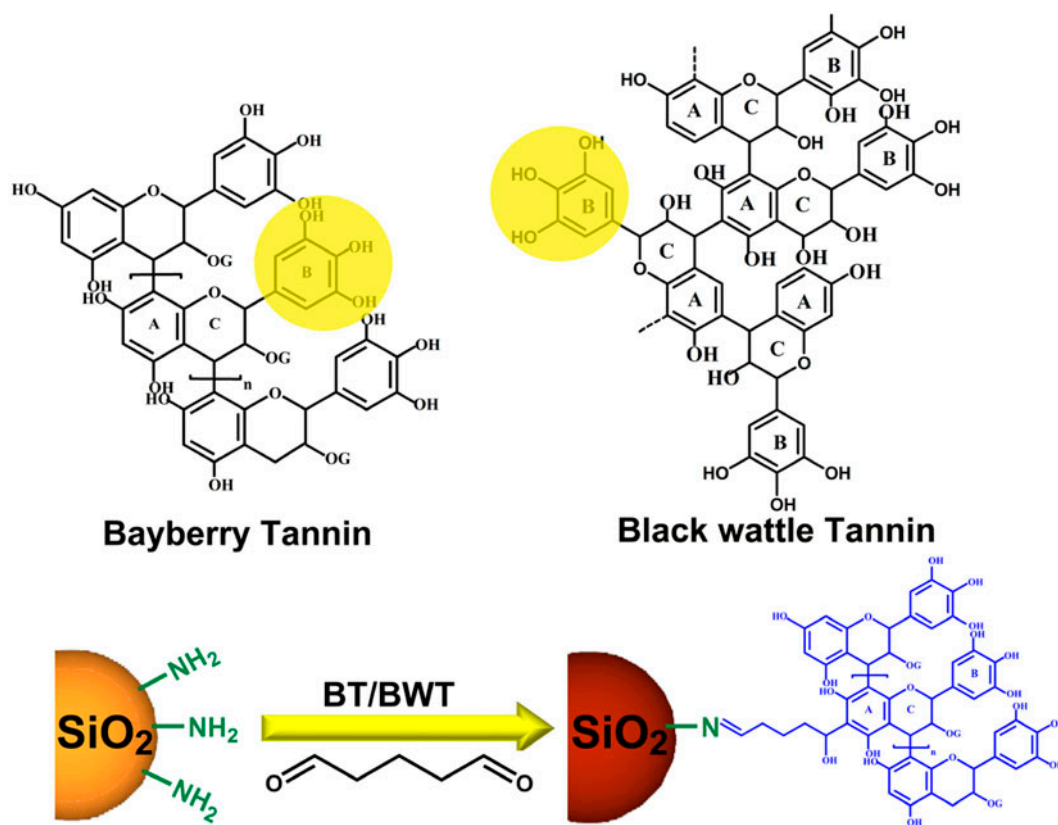


Fig. 1. Molecular structures of bayberry tannin (BT) and black wattle tannin (BWT) and synthesis route of  $\text{SiO}_2$ -BT/BWT.

terized by Fourier transform infrared spectroscopy (FTIR, Nicolet 2005).

## 2.2. Preparation of adsorbents

### 2.2.1. Preparation of aminated silica ( $\text{NH}_2\text{-SiO}_2$ )

Aminated silica was prepared according to the literature [22]. Cyclohexane was dissolved in hexanol mixed with Triton X-100 (4:1:1, V:V) in a round-bottom flask. Then mixture was stirred at 40°C for 30 min. After adding 5 mL of deionized water, the mixture was stirred at 40°C for 30 min (10: 1, deionized water: Triton X-100). And the mixed solution of TEOS (5 mL) and silane coupling agent (KH-550) was added into the mixture and stirred at 40°C for another 30 min. Then 2 mL of  $\text{NH}_3\text{-H}_2\text{O}$  was added and stirred at 40°C for 24 h. Subsequently, the product was washed with deionized water and dried in vacuum at 40°C for 24 h to obtain  $\text{NH}_2\text{-SiO}_2$ .

### 2.2.2. Preparation of the adsorbents ( $\text{SiO}_2\text{-BT}$ , $\text{SiO}_2\text{-BWT}$ )

About 1.0 g BT was dissolved in 100 mL of deionized water, then the solution was mixed with the  $\text{NH}_2\text{-SiO}_2$  prepared above. Ten milliliters of glutaraldehyde (20.0 wt.%) solution was added into the mixture, and was stirred at 40°C for 6 h. The initial pH of the mixture was adjusted to 2.0 with  $\text{HNO}_3$  (0.1 mol/L), then the mixture was stirred at 40°C for 24 h. After reaction, the product was washed with deionized water and dried in vacuum at 40°C for 24 h to obtain  $\text{SiO}_2\text{-BT}$  adsorbent. The preparation of  $\text{SiO}_2\text{-BWT}$  was the same as the  $\text{SiO}_2\text{-BT}$  (Fig. 1 synthesis route of  $\text{SiO}_2\text{-BT/BWT}$ ).

## 2.3. Adsorption experiments ( $\text{Pr}^{3+}$ and $\text{Nd}^{3+}$ mixed aqueous solution system)

### 2.3.1. Effect of initial pH on adsorption capacity of the adsorbents

About 0.1 g of the adsorbent ( $\text{SiO}_2\text{-BT}$ ,  $\text{SiO}_2\text{-BWT}$ ) was suspended in 50 mL of  $\text{Pr}^{3+}$  and  $\text{Nd}^{3+}$  mixed aqueous solutions, respectively. The concentrations of  $\text{Pr}^{3+}$  and  $\text{Nd}^{3+}$  were 2.0 mmol/L and the initial pH of the solutions ranged from 1.0 to 6.0. The adsorption process was conducted at 40°C with constant shaking for 1 h. When the adsorption was completed, the suspension was filtered by the filter with a diameter of 0.45  $\mu\text{m}$  and the concentration of  $\text{Pr}^{3+}$  and  $\text{Nd}^{3+}$  in the filtrate was analyzed by ICP-OES. The adsorption

capacity ( $q_e$ , mg/g) of  $\text{SiO}_2\text{-BT}$  and  $\text{SiO}_2\text{-BWT}$  to  $\text{Pr}^{3+}$  and  $\text{Nd}^{3+}$  was obtained by mass balance calculations.

### 2.3.2. Adsorption isotherms

About 0.1 g of adsorbent ( $\text{SiO}_2\text{-BT}$ ,  $\text{SiO}_2\text{-BWT}$ ) was suspended in 50 mL of  $\text{Pr}^{3+}$  and  $\text{Nd}^{3+}$  mixed aqueous solutions with initial concentration ranging from 1.8 to 6.0 mmol/L. The pH of  $\text{Pr}^{3+}$  and  $\text{Nd}^{3+}$  mixed aqueous solution was adjusted to 5.0. The adsorption experiments were conducted by constant shaking at 40°C for 1 h. Then the suspension was filtered and the concentration of  $\text{Pr}^{3+}$  and  $\text{Nd}^{3+}$  mixed in the filtrate was analyzed by ICP-OES, respectively.

### 2.3.3. Dynamic adsorption and desorption experiments

Two grams of adsorbent ( $\text{SiO}_2\text{-BT}$ ,  $\text{SiO}_2\text{-BWT}$ ) was suspended in the adsorption column (10  $\times$  300 mm), respectively. The column was equilibrated with water (pH 5).  $\text{Pr}^{3+}$  and  $\text{Nd}^{3+}$  mixed solution (1.8 mmol/L, pH 5) was pumped into the column with a constant velocity of 2.0 BV/h (BV = bed volume). The effluent was collected by an automatic collector and the concentration of the effluent was analyzed by ICP-OES. After reaching the adsorption equilibrium, the column was eluted by 0.1 mol/L  $\text{HNO}_3$  solution at 2.0 BV/h, and the eluent was collected for  $\text{Pr}^{3+}$  and  $\text{Nd}^{3+}$  analysis.

## 2.4. Simulation of real smelting water system

### 2.4.1. Effect of initial pH on adsorption capacity of the adsorbents

About 0.1 g of adsorbent ( $\text{SiO}_2\text{-BT}$ ,  $\text{SiO}_2\text{-BWT}$ ) was suspended in 20 mL of simulated real smelting water, respectively. The pH of the solutions ranged from 2.0 to 5.0. The adsorption process was conducted at 40°C with constant stirring for 40 min. When the adsorption was completed, the suspension was filtered and the concentrations of  $\text{La}^{3+}$ ,  $\text{Ce}^{3+}$ ,  $\text{Pr}^{3+}$ , and  $\text{Nd}^{3+}$  in the filtrate were analyzed by ICP-OES. By calculating the difference of the solutions before and after adsorption of  $\text{La}^{3+}$ ,  $\text{Ce}^{3+}$ ,  $\text{Pr}^{3+}$ , and  $\text{Nd}^{3+}$ , the total amount of variability is obtained under different pH on adsorption capacity of  $q_e$  ( $q_e$ , mg/g).

### 2.4.2. Effect of temperature on adsorption capacity of the adsorbents

About 0.1 g of adsorbent ( $\text{SiO}_2\text{-BT}$ ,  $\text{SiO}_2\text{-BWT}$ ) was suspended in 20 mL of simulated real smelting water,

respectively. The pH of simulated real smelting water was adjusted to 4.0. The adsorption experiments were conducted by constant shaking at 30, 40, 50, and 60 °C for 40 min, respectively. Then the suspensions were filtered and the concentrations of  $\text{La}^{3+}$ ,  $\text{Ce}^{3+}$ ,  $\text{Pr}^{3+}$ , and  $\text{Nd}^{3+}$  mixed in the filtrate was analyzed.

#### 2.4.3. Effect of time on adsorption capacity of the adsorbents

About 0.1 g of adsorbent ( $\text{SiO}_2\text{-BT}$ ,  $\text{SiO}_2\text{-BWT}$ ) was suspended in 20 mL of simulated real smelting water respectively. The pH of simulated real smelting water was adjusted to 4.0. The adsorption experiments were conducted by constant shaking at 40 °C for 40 min. Then the suspension was filtered and the concentration of  $\text{Pr}^{3+}$  and  $\text{Nd}^{3+}$  in the filtrate was analyzed.

### 3. Results and discussions

#### 3.1. Characterization of adsorbents

The SEM micrographs spectra of  $\text{NH}_2\text{-SiO}_2$ ,  $\text{SiO}_2\text{-BT}$ , and  $\text{SiO}_2\text{-BWT}$  are shown in Fig. 2(a), (b), and (c). The particle morphology of  $\text{SiO}_2\text{-BT}$  and  $\text{SiO}_2\text{-BWT}$

has no significant changes after being modified by plant tannin compared with  $\text{NH}_2\text{-SiO}_2$ .

FTIR spectra of the  $\text{NH}_2\text{-SiO}_2$ ,  $\text{SiO}_2\text{-BT}$ , and  $\text{SiO}_2\text{-BWT}$  were shown as Fig. 2(d) ((1)–(3)). The absorption band at  $1,059.88\text{ cm}^{-1}$  in (1) is due to stretching vibration of structural Si–O–Si of  $\text{NH}_2\text{SiO}_2$  and the bands at  $461.18\text{ cm}^{-1}$  is attributed to the Si–O–Si bending vibration [22]. The band at  $3,424.47\text{ cm}^{-1}$  is assigned to the bending vibration of –OH on the surface of silica. The absorption band at  $788.83\text{ cm}^{-1}$  is attributed to the Si–OH stretching vibration. All of the data above indicated that the silica was successfully modified by amino groups.

The FTIR spectra of  $\text{SiO}_2\text{-BT}$  and  $\text{SiO}_2\text{-BWT}$  are shown in Fig. 2(d), (2) and (3), respectively. The major absorption bands at  $1,073.26$  and  $1,073.93\text{ cm}^{-1}$  are assigned to asymmetric stretching vibration of structural Si–O–Si (in  $\text{NH}_2\text{-SiO}_2$ ), and the bands at  $462.28$  and  $461.23\text{ cm}^{-1}$  are attributed to the Si–O–Si bending vibration. The bands at  $3,410.95$  and  $3,409.44\text{ cm}^{-1}$  are due to the phenolic hydroxyl (in the molecule of BT and BWT) stretching vibration and the –OH (in  $\text{NH}_2\text{-SiO}_2$ ) stretching vibration. The bands at  $1,627.60$  and  $1,507.85\text{ cm}^{-1}$  indicate the benzene skeleton vibration of tannin structure [22]. As it is shown, the bands at  $2,940.96$  and  $2,942.72\text{ cm}^{-1}$  are stretching vibration

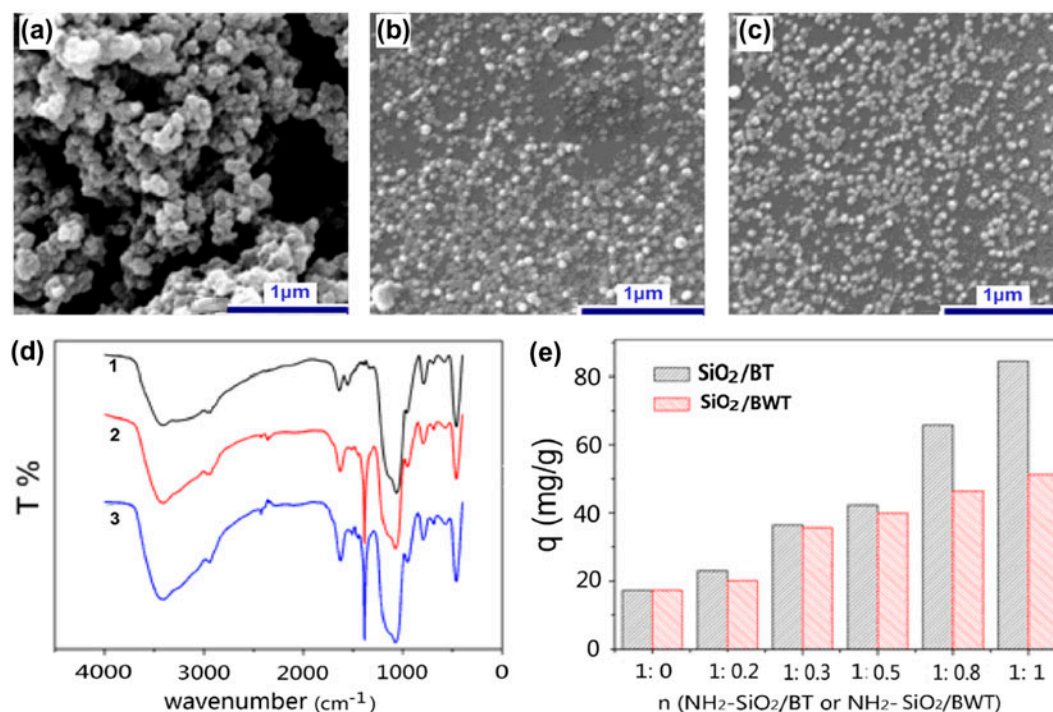


Fig. 2. SEM images of (a)  $\text{NH}_2\text{-SiO}_2$ , (b)  $\text{SiO}_2\text{-BT}$ , (c)  $\text{SiO}_2\text{-BWT}$ , (d) FTIR image of (1)  $\text{NH}_2\text{-SiO}_2$ , (2)  $\text{SiO}_2\text{-BT}$ , and (3)  $\text{SiO}_2\text{-BWT}$ , and (e) Effect on the adsorption capacity of  $\text{Pr}^{3+}$  aqueous solutions with different grafting tannin content.

characteristics of saturated absorption peak of C–H bond. These analysis results showed that the tannins were grafted onto the aminated  $\text{SiO}_2$ .

Fig. 2(e) shows the influence of grafting tannin quality ratio on the adsorption capacity of  $\text{SiO}_2$ -BT and  $\text{SiO}_2$ -BWT to  $\text{Pr}^{3+}$  aqueous solution. Pure  $\text{NH}_2$ - $\text{SiO}_2$  exhibited low adsorption capacity and low efficiency, which was about 10 mg/g. The adsorption capacity of  $\text{Pr}^{3+}$  improved gradually with the increase in tannin content. It can be explained that the adsorption of as-prepared adsorbents to  $\text{Pr}^{3+}$  was realized by the formation of five-member chelating ring between  $\text{Pr}^{3+}$  and phenolic hydroxyl in tannin. The amount of phenolic hydroxyls increased with increasing tannin amount. In the subsequent experiments, the quality ratio was fixed as 1:1.

### 3.2. Adsorption performance of the adsorbents in $\text{Pr}^{3+}$ and $\text{Nd}^{3+}$ mixed aqueous solutions system

#### 3.2.1. Effect of initial pH on adsorption capacity of the adsorbents

Fig. 3(a) shows the influence of initial pH on the adsorption capacity of  $\text{SiO}_2$ -BT and  $\text{SiO}_2$ -BWT to  $\text{Pr}^{3+}$  and  $\text{Nd}^{3+}$  in  $\text{Pr}^{3+}$  and  $\text{Nd}^{3+}$  mixed aqueous solutions systems. There was a significant competitive adsorption between the  $\text{Pr}^{3+}$  and  $\text{Nd}^{3+}$  on both the adsorbents. The adsorption capacities on  $\text{Pr}^{3+}$  and  $\text{Nd}^{3+}$  significantly increased when the pH increased from 1.0 to 5.0. When adjusting the pH to 6.0, the adsorption capacities on  $\text{Pr}^{3+}$  and  $\text{Nd}^{3+}$  decreased slightly. This result was attributed to the influence of pH on the dissociation degree of phenolic hydroxyls in BT and BWT [23]. When the pH of the solution was low,

$\text{H}^+$  with high concentrations have restrained the dissociation of phenolic hydroxyl, resulting in a low adsorption capacity of  $\text{Pr}^{3+}$  and  $\text{Nd}^{3+}$ . In a solution with higher pH, the dissociation of phenolic hydroxyls in BT and BWT will be promoted, which was beneficial for chelating REIs. However, excess  $-\text{OH}$  in the solution often leads to hydrolysis of  $\text{Pr}^{3+}$  and  $\text{Nd}^{3+}$  or the oxidation of tannin [24], resulting in lower adsorption capacity of  $\text{Pr}^{3+}$  and  $\text{Nd}^{3+}$ . The optimal pH for adsorption of  $\text{SiO}_2$ -BT and  $\text{SiO}_2$ -BWT on  $\text{Pr}^{3+}$  and  $\text{Nd}^{3+}$  which could reach the maximum capacity were 5.0 and 4.0, respectively. Both the adsorbents showed better adsorption capacity to  $\text{Nd}^{3+}$  than that of  $\text{Pr}^{3+}$ . Moreover,  $\text{SiO}_2$ -BT exhibited a higher adsorption capacity than  $\text{SiO}_2$ -BWT, probably because of potential active functional groups of BT.

#### 3.2.2. Adsorption isotherms

The influence of initial concentration of  $\text{Pr}^{3+}$  and  $\text{Nd}^{3+}$  on the capacities of the two adsorbents is indicated in Fig. 3(b). The initial concentration of  $\text{Pr}^{3+}$  and  $\text{Nd}^{3+}$  was in the range of 1.8–6.0 mmol/L. The adsorption amounts of adsorbents to  $\text{Pr}^{3+}$  and  $\text{Nd}^{3+}$  in the mixed system increased along with the increasing concentrations. Both the adsorbents showed higher adsorption capacity with higher concentration. Under the conditions of  $C = 6.0$  mmol/L, pH 5.0 ( $\text{SiO}_2$ -BT), 4.0 ( $\text{SiO}_2$ -BWT), and  $T = 40^\circ\text{C}$ , the difference in adsorption capacity of the  $\text{SiO}_2$ -BT on the  $\text{Pr}^{3+}$  and  $\text{Nd}^{3+}$  was up to 236.63 mg/g, and the difference in adsorption capacity of the  $\text{SiO}_2$ -BWT on the  $\text{Pr}^{3+}$  and  $\text{Nd}^{3+}$  could reach 190.20 mg/g, showing significant competitive adsorption between  $\text{Pr}^{3+}$  and  $\text{Nd}^{3+}$ .

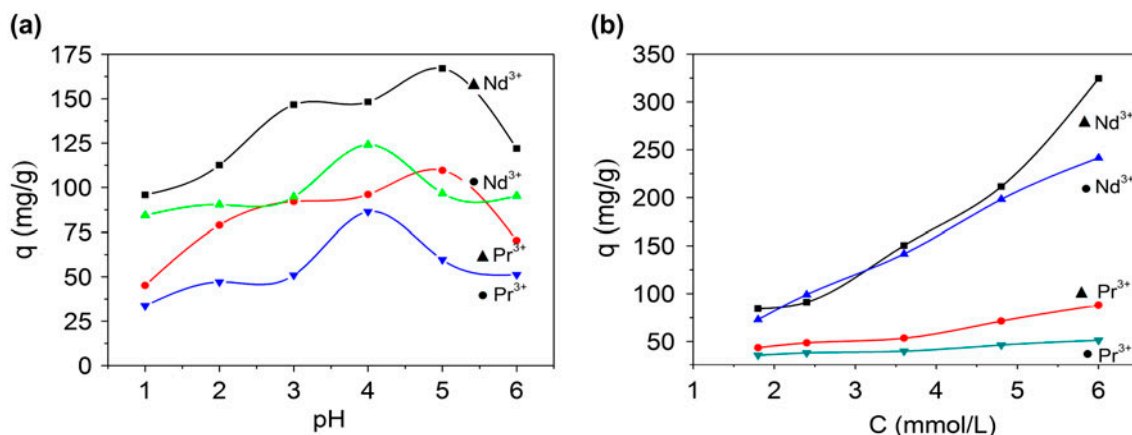


Fig. 3. Effect of initial pH (a) and concentration (b) on the adsorption capacity of  $\text{Pr}^{3+}$  and  $\text{Nd}^{3+}$  in the mixed concentrations on these adsorbents ( $\blacktriangle$ ,  $\text{SiO}_2$ -BT;  $\bullet$ ,  $\text{SiO}_2$ -BWT).

Adsorption isotherms data were further fitted by Freundlich isothermal equations. The experimental data could be fitted by the classical Freundlich equation. The Freundlich equation is expressed as follows [25]:

$$\ln(q_e) = 1/n \ln(C_e) + \ln(K_F) \quad (1)$$

where  $q_e$  is the adsorption capacity of  $\text{Pr}^{3+}$  and  $\text{Nd}^{3+}$  at equilibrium (mg/g),  $C_e$  is the concentration of  $\text{Pr}^{3+}$  and  $\text{Nd}^{3+}$  at equilibrium (mmol/L),  $K_F$  and  $n$  are the Freundlich constants related to adsorption capacity and adsorption intensity, respectively. The Freundlich models fitting results were summarized in Table 1.

As shown in Table 1, the Freundlich equation gave satisfied fitting to the isotherm data with correlation constant ( $R^2$ ) higher than 0.90, and the theoretical adsorption capacities were close to those determined by experiments. All these results suggested that  $\text{Pr}^{3+}$  and  $\text{Nd}^{3+}$  may be adsorbed in the form of multi-layer on the surface of the adsorbents ( $\text{SiO}_2\text{-BT}$ ,  $\text{SiO}_2\text{-BWT}$ ).

Freundlich equation parameter  $1/n$  is a constant related to the adsorption force. Smaller value of  $1/n$  in Table 1 meant stronger adsorption, indicating that the adsorption of  $\text{Pr}^{3+}$  and  $\text{Nd}^{3+}$  by the two adsorbents ( $\text{SiO}_2\text{-BT}$ ,  $\text{SiO}_2\text{-BWT}$ ) can be carried out under mild conditions.

### 3.2.3. Adsorption kinetics

The adsorption kinetics of  $\text{Pr}^{3+}$  and  $\text{Nd}^{3+}$  on the two adsorbents ( $\text{SiO}_2\text{-BT}$ ,  $\text{SiO}_2\text{-BWT}$ ) is illustrated in Fig. 4(a) and (b). The adsorption capacity of  $\text{Pr}^{3+}$  and  $\text{Nd}^{3+}$  sharply increased with the increase in contact time at the beginning of the adsorption process (0–40 min), and then gradually reached an equilibrium value in approximately 60 min. The initial concentration of  $\text{Pr}^{3+}$  and  $\text{Nd}^{3+}$  showed no significant effect on the time to attain adsorption equilibrium. Therefore, the adsorption of  $\text{Pr}^{3+}$  and  $\text{Nd}^{3+}$  should take place at the outer surface of the two adsorbents and the intra-

particle diffusion resistance could be neglected. To further investigate the adsorption process, pseudo-second-order rate models were used to fit the adsorption kinetic data. The pseudo-second-order rate [26] (2) model is given as follows:

$$T/q_t = 1/(k_2 q_e^2) + t/q_e \quad (2)$$

where  $q_e$  and  $q_t$  are the amount of  $\text{Pr}^{3+}$  and  $\text{Nd}^{3+}$  adsorbed (mg/g) at equilibrium and at time  $t$  (min), respectively, and  $k_2$  is the rate constant of the pseudo-second-order rate model (mg/g min). The absorption reaction was in accordance with the pseudo-second-order kinetic equation (Table 2), and it could be considered as the chemical adsorption reaction.

### 3.2.4. Effect of initial temperature on adsorption capacity

Effect of temperature on the adsorption of  $\text{Pr}^{3+}$  and  $\text{Nd}^{3+}$  is shown in Fig. 4(b) and (d). The effect of temperature on the adsorption capacity was not obvious. Adsorption among two REIs, the optimal temperature for high adsorption capacity of  $\text{Nd}^{3+}$  and  $\text{Pr}^{3+}$  was 40°C. The best adsorption temperature for  $\text{SiO}_2\text{-BWT}$  on  $\text{Nd}^{3+}$  was 50°C.

$$\ln C_e = \Delta H/(RT) + \ln K$$

$$\Delta H = 510.06 \text{ KJ/mol}$$

The  $C_e$  is adsorption equilibrium concentration (mmol/L) of different initial concentration.  $R$ ,  $T$ ,  $\Delta H$ , and  $K$  are adsorption isotherms related to gas constant, the absolute temperature and enthalpy value, and constant, respectively. The enthalpy change of the adsorption process with the  $\ln C_e - 1/T$  plot can be plotted at different temperatures. If  $\Delta H > 40 \text{ KJ/mol}$ , it indicates that it was an endothermic reaction and the adsorption increased with increasing temperature [27].

### 3.2.5. Column of adsorbents

The breakthrough curve of  $\text{Pr}^{3+}$  and  $\text{Nd}^{3+}$  mixed aqueous solutions on the column is shown in Fig. 5(a). When the effluent volume was 240.0 mL, the two adsorbents basically reached the saturation adsorption. Almost all of the  $\text{Pr}^{3+}$  and  $\text{Nd}^{3+}$  in the mixed solution were absorbed by the adsorbents. The desorption curve is shown in Fig. 5(b). When the concentration was 6 mmol/L, the adsorption rate of  $\text{Nd}^{3+}$  and  $\text{Pr}^{3+}$  on

Table 1  
The Freundlich model parameters of the adsorption of  $\text{Pr}^{3+}$  and  $\text{Nd}^{3+}$  in the mixed concentrations on these adsorbents

Adsorbents	RE <sup>3+</sup>	Freundlich		
		$R^2$	$K_F$	$1/n$
$\text{SiO}_2\text{-BT}$	$\text{Pr}^{3+}$	0.92	29.54	0.57
	$\text{Nd}^{3+}$	0.96	38.08	1.13
$\text{SiO}_2\text{-BWT}$	$\text{Pr}^{3+}$	0.93	29.33	0.30
	$\text{Nd}^{3+}$	0.99	40.78	0.99

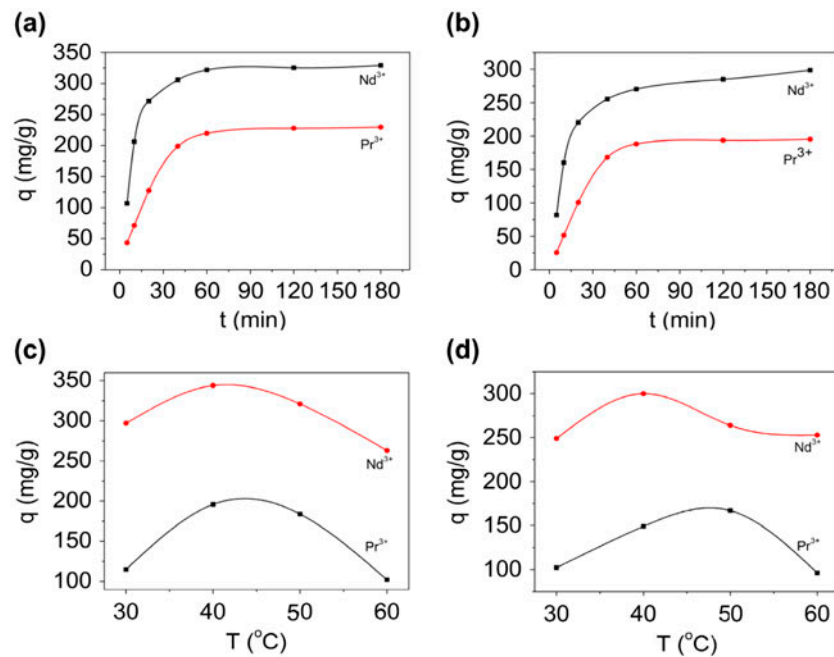


Fig. 4. Adsorption kinetics and effect of initial temperature on the adsorption capacity of rare earth solution ( $\text{Pr}^{3+}$ ,  $\text{Nd}^{3+}$ ) on  $\text{SiO}_2\text{-BT}$  (a, c),  $\text{SiO}_2\text{-BWT}$  (b, d).

Table 2  
The parameters of pseudo-second-order model

Adsorbents	RE <sup>3+</sup>	$q_e$ (calculated value) (mg/g)	$q_e$ (measured value) (mg/g)	Er	$k_2$ (g/mg min)	$R^2$
$\text{SiO}_2\text{-BT}$	$\text{Nd}^{3+}$	332.40	329.20	0.0097	$3.84 \times 10^{-3}$	0.99
	$\text{Pr}^{3+}$	298.70	290.90	0.027	$4.07 \times 10^{-3}$	0.83
$\text{SiO}_2\text{-BWT}$	$\text{Nd}^{3+}$	300.30	298.60	0.0058	$2.80 \times 10^{-3}$	0.99
	$\text{Pr}^{3+}$	205.60	193.70	0.068	$8.33 \times 10^{-3}$	0.93

Note:  $\text{Er} = [q_e (\text{calculated value}) - q_e (\text{measured value})] / q_e (\text{measured value})$  (mg/g).

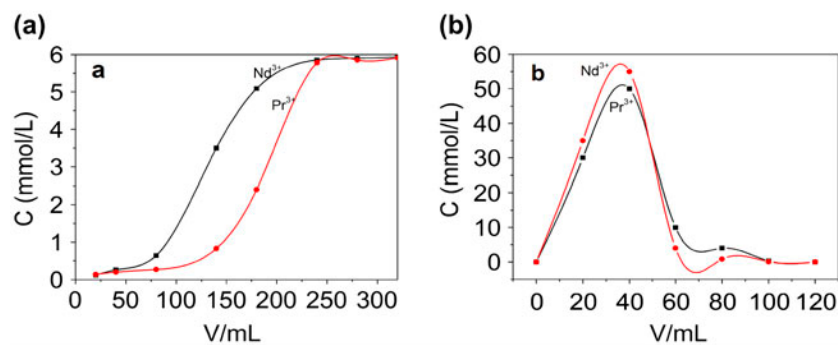


Fig. 5. (a) the adsorption of  $\text{Pr}^{3+}$  and  $\text{Nd}^{3+}$  breakthrough curves and (b) the elution of  $\text{HNO}_3$  desorption curve.

$\text{SiO}_2\text{-BT}$  could reach 76.82 and 20.36%, respectively. Subsequently, the adsorbents column was desorbed by  $\text{H}_2\text{O}$ , alcohol and 0.1 mol/L  $\text{HNO}_3$  solutions, respectively. The

REIs could not be eluted by alcohol and  $\text{H}_2\text{O}$ . However, the resolution rate could reach 98.00% by 0.1 mol/L  $\text{HNO}_3$  solution, showing satisfied reusability.

### 3.3. Adsorption performance in simulated real smelting water system ( $\text{La}^{3+}$ , $\text{Ce}^{3+}$ , $\text{Pr}^{3+}$ , $\text{Nd}^{3+}$ )

#### 3.3.1. Effect of initial pH on adsorption capacity of the adsorbents

Fig. 6(a) and (b) shows the influence of initial pH on the adsorption capacity of adsorbents ( $\text{SiO}_2\text{-BT}$ ,  $\text{SiO}_2\text{-BWT}$ ) in simulated real smelting water. The adsorption capacity increased significantly when the pH increased from 2.0 to 4.0. When the pH was 5.0 ( $\text{SiO}_2\text{-BT}$ ) and 4.0 ( $\text{SiO}_2\text{-BWT}$ ), the adsorption capacity of the two adsorbents reached the maximum value, the result was the same as the one in the mixed solutions system ( $\text{Pr}^{3+}$ ,  $\text{Nd}^{3+}$ ). When the pH was increased from 2.0 to 5.0, the adsorption capacity of the two adsorbents on  $\text{La}^{3+}$  and  $\text{Ce}^{3+}$  increased obviously while the adsorption capacity on  $\text{Pr}^{3+}$  and  $\text{Nd}^{3+}$  increased slightly. A higher pH was beneficial for the adsorption of  $\text{La}^{3+}$  and  $\text{Ce}^{3+}$ . However,  $\text{La}^{3+}$ ,  $\text{Ce}^{3+}$ ,  $\text{Pr}^{3+}$ , and  $\text{Nd}^{3+}$  would precipitate under the pH higher than 5.0.

#### 3.3.2. Effect of initial temperature on adsorption capacity of the adsorbents

Effect of temperature on the adsorption of  $\text{La}^{3+}$ ,  $\text{Ce}^{3+}$ ,  $\text{Pr}^{3+}$ , and  $\text{Nd}^{3+}$  is shown in Fig. 6(c) and (d). The effect of temperature on adsorption capacity was not

obvious. Adsorption among these four REIs, the optimal temperature for high absorption capacity of  $\text{La}^{3+}$ ,  $\text{Ce}^{3+}$ , and  $\text{Pr}^{3+}$  was  $40^\circ\text{C}$ . The best adsorption temperature for  $\text{SiO}_2\text{-BWT}$  on  $\text{Nd}^{3+}$  was  $50^\circ\text{C}$ .

#### 3.3.3. Effect of initial time on adsorption capacity of the adsorbents

Fig. 6(e) and (f) indicates that the two adsorbents showed higher adsorption capacity with prolonged adsorption time on the four REIs ( $\text{La}^{3+}$ ,  $\text{Ce}^{3+}$ ,  $\text{Pr}^{3+}$ , and  $\text{Nd}^{3+}$ ), which could achieve equilibrium adsorption in about 50 min. At the beginning of the adsorption process, adsorption capacity increased fast. A possible reason was the suitable pH on which rare earth ion concentration and adsorbent of surfactant adsorption sites were beneficial for the fast adsorption of  $\text{RE}^{3+}$ . Along with the process of adsorption, tannin dissociation has produced a large amount of  $\text{H}^+$  into the solution, leading to a lower pH. Furthermore, the light rare earth ion concentration in the solution and the adsorbent surface active adsorption sites reduced during the adsorption process. The three reasons above would result in adsorption capacity growth slowly and finally achieve the balance.

As shown in Table 3, the Freundlich equation gave poor fitting to the isotherm data with correlation constant ( $R^2$ ) lower than 0.5, and the theoretical adsorption

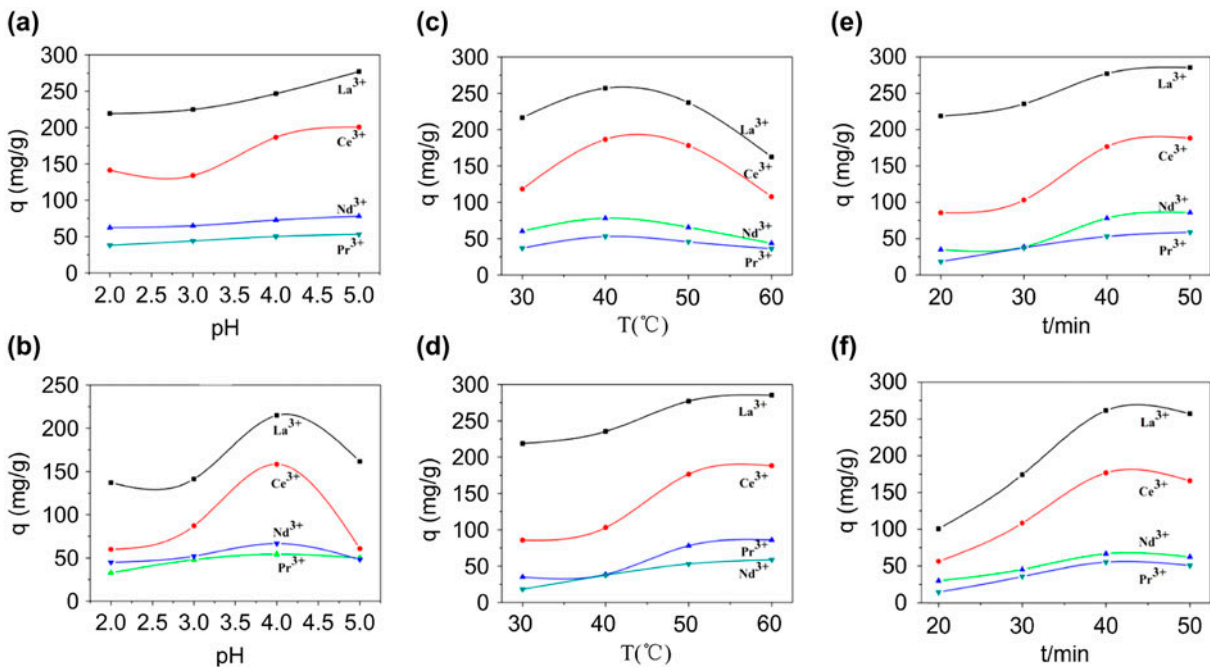


Fig. 6. Effect of initial pH, temperature and time on  $\text{SiO}_2\text{-BT}$  (a, c, e) and  $\text{SiO}_2\text{-BWT}$  (b, d, f) adsorbents in simulated real smelting water ( $\text{La}^{3+}$ ,  $\text{Ce}^{3+}$ ,  $\text{Nd}^{3+}$ ,  $\text{Pr}^{3+}$ ).

Table 3

The Freundlich model parameters of the adsorption of simulated real smelting water on the adsorbents

Adsorbents	RE <sup>3+</sup>	$q_e$ (calculated value) (mg/g)	$q_e$ (measured value) (mg/g)	Er	$k_2$ (g/mg min)	$R^2$
SiO <sub>2</sub> -BT	La <sup>3+</sup>	285.25	284.58	0.0024	$1.79 \times 10^{-4}$	0.98
	Ce <sup>3+</sup>	188.13	193.87	-0.029	$2.18 \times 10^{-8}$	0.019
	Nd <sup>3+</sup>	86.01	65.88	0.31	$6.78 \times 10^{-6}$	0.44
	Pr <sup>3+</sup>	58.78	72.39	-0.19	$3.99 \times 10^{-7}$	0.069
SiO <sub>2</sub> -BWT	La <sup>3+</sup>	256.96	262.61	-0.022	$1.71 \times 10^{-8}$	0.035
	Ce <sup>3+</sup>	166.01	138.50	0.20	$1.60 \times 10^{-6}$	0.26
	Nd <sup>3+</sup>	62.58	613.49	-0.90	$8.69 \times 10^{-9}$	0.091
	Pr <sup>3+</sup>	50.81	63.24	-0.20	$2.25 \times 10^{-4}$	0.34

Note: Er =  $[q_e$  (calculated value) -  $q_e$  (measured value)]/ $q_e$  (measured value) (mg/g).

capacities were not close to those determined by experiments. All these results suggested that the adsorption of SiO<sub>2</sub>-BT has followed pseudo-second-order kinetic and indicated a better selectivity to La<sup>3+</sup> [28]. However, the simulated adsorption of the two adsorbents in simulated real smelting water didn't conform to pseudo-second-order kinetic and fitting parameter didn't conform to pseudo-second-order kinetic. The reason was that there was an adsorption competition on the two adsorbents in the adsorption of the four REIs [29,30]. The selectivity of the four REIs on the two adsorbents is shown as follows: La<sup>3+</sup> > Ce<sup>3+</sup> > Nd<sup>3+</sup> > Pr<sup>3+</sup>.

#### 4. Conclusions

In this study, aminated silica BT (SiO<sub>2</sub>-BT) and aminated silica BWT (SiO<sub>2</sub>-BWT) have been successfully prepared and applied for adsorbing mixed REIs aqueous solutions. The result showed the two adsorbents exhibited better adsorption capacity to Nd<sup>3+</sup> than that of Pr<sup>3+</sup> and SiO<sub>2</sub>-BT exhibited a higher adsorption capacity than SiO<sub>2</sub>-BWT. The adsorption kinetics was in accordance with the pseudo-second-order rate equations and the resolution rate could reach 98.00% by 0.1 mol/L HNO<sub>3</sub> solution, the reaction was the endothermic and chemical adsorption reaction. The selectivity of the four REIs on the two adsorbents is shown as follows: La<sup>3+</sup> > Ce<sup>3+</sup> > Nd<sup>3+</sup> > Pr<sup>3+</sup>. The SiO<sub>2</sub>-BT and SiO<sub>2</sub>-BWT exhibited best selectivity to La<sup>3+</sup> among these four REIs (La<sup>3+</sup>, Ce<sup>3+</sup>, Pr<sup>3+</sup>, Nd<sup>3+</sup>).

#### Acknowledgment

This research was financially supported by the National Natural Science Foundation of China (51173122, 21406147) and Science and Technology Project of Chengdu (2014-HM01-00204-SF; 2014-HM01-00205-SF).

#### References

- [1] L.T. Peiró, G.V. Méndez, Material and energy requirement for rare earth production, *JOM* 65 (2013) 1327–1340.
- [2] B.Q. Yang, X.P. Zhang, Analysis of global rare earth production and consumption of the light rare earth elements and thorium in baotou iron ore by a micro-column, *J. Radioanal. Nucl. Chem.* 281 (2009) 647–654.
- [3] T. Liang, K.X. Li, L.Q. Wang, State of rare earth elements in different environmental components in mining areas of China, *Environ. Monit. Assess.* 186 (2014) 1499–1513.
- [4] S.R. Chi, Z. Zhou, Z. Xu, Y. Hu, G. Zhu, S. Xu, Solution-chemistry analysis of ammonium bicarbonate consumption in rare-earth-element precipitation, *Metall. Mater. Trans. B* 34 (2003) 611–617.
- [5] A. Ikeda, T. Suzuki, M. Aida, Y. Fujii, T. Mitsugashira, M. Hara, M. Ozawa, Chromatographic separation of trivalent actinides and rare earth elements by using pyridine type resin, *J. Radioanal. Nucl. Chem.* 263 (2005) 605–611.
- [6] Y. Tomobuchi, Y. Tachibana, M. Nomura, T. Suzuki, Effect of alcohols on separation behavior of rare earth elements using benzimidazole-type anion-exchange resin in nitric acid solutions, *J. Radioanal. Nucl. Chem.* 303 (2015) 1425–1428.
- [7] P. Zaheri, H. Abolghasemi, T. Mohammadi, M.G. Maraghe, Synergistic extraction and separation of dysprosium and europium by supported liquid membrane, *Chem. Eng. J.* 8 (2015) 1642–1648.
- [8] F.N. Behdani, A.T. Rafsanjani, M. Torab-Mostaedi, Adsorption ability of oxidized multiwalled carbon nanotubes towards aqueous Ce(III) and Sm(III), *Korean J. Chem. Eng.* 30 (2013) 448–455.
- [9] R. Qadeer, Adsorption of neodymium ions on activated charcoal from aqueous solutions, *J. Radioanal. Nucl. Chem.* 265 (2005) 377–381.
- [10] A. Jordens, Y.P. Cheng, K.E. Waters, A review of the beneficiation of rare earth element bearing minerals, *Miner. Eng.* 41 (2013) 97–114.
- [11] K. Inoue, S. Alam, Refining and mutual separation of rare earths using biomass wastes, *JOM* 65 (2013) 1341–1347.
- [12] B. Dhir, Potential of biological materials for removing heavy metals from wastewater, *Environ. Sci. Pollut. Res.* 21 (2014) 1614–1627.

- [13] F. Goecke, V. Zachleder, M. Vítová, *Algal Biorefineries, Rare Earth Elements and Algae: Physiological Effects, Biorefinery and Recycling*, Springer International Publishing, Switzerland, 2015.
- [14] A. Minoda, H. Sawada, S. Suzuki, S. Miyashita, K. Inagaki, T. Yamamoto, M. Tsuzuki, Recovery of rare earth elements from the sulfothermophilic red alga *Galdieria sulphuraria* using aqueous acid, *Appl. Microbiol. Biotechnol.* 99 (2015) 1513–1519.
- [15] H. Moriwaki, H. Yamamoto, Interactions of microorganisms with rare earth ions and their utilization for separation and environmental technology, *Appl. Microbiol. Biotechnol.* 97 (2013) 1–8.
- [16] S. Abadian, A. Rahbar-Kelishami, R. Norouzbeigi, M. Peydayesh, Cu (II) adsorption onto platanus orientalis leaf powder: Kinetic, isotherm, and thermodynamic studies, *Res. Chem. Intermed.* 41 (2015) 669–7681.
- [17] Y.V. Larichev, P.M. Eletsii, F.V. Tuzikov, V.A. Yakovlev, Porous carbon-silica composites and carbon materials from rice husk: Production technology, texture, and dispersity, *Catal. Ind.* 5 (2013) 350–357.
- [18] M. Kavand, T. Kaghazchi, M. Soleimani, Optimization of parameters for competitive adsorption of heavy metal ions ( $Pb^{2+}$ ,  $Ni^{2+}$ ,  $Cd^{2+}$ ) onto activated carbon, *Korean J. Chem. Eng.* 31 (2014) 692–700.
- [19] C.W. Cheung, K.K.H. Choy, J.F. Porter, Removal of cadmium (II) from aqueous solution by agricultural waste cashew nut shell, *Korean J. Chem. Eng.* 29 (2012) 756–768.
- [20] X. Liu, H.Y. Ao, X. Xiong, J.G. Xiao, J.T. Liu, Arsenic Removal from Water by Iron-Modified Bamboo Charcoal, *Water Air Soil Pollut.* 223 (2012) 1033–1044.
- [21] J.W. Gooch, Tannin, *Encyclopedic Dictionary of Polymers*, 2011.
- [22] X. Huang, X.P. Liao, B. Shi, Tannin-immobilized mesoporous silica bead (BT-SiO<sub>2</sub>) as an effective adsorbent of Cr(III) in aqueous solution, *J. Hazard. Mater.* 173 (2010) 33–39.
- [23] A.L. Uğur, M.Ü. Özgür, G. Gümrükçü, *Innovations in Chemical Biology*, Springer, Netherlands, 2009.
- [24] X.P. Liao, L. Li, B. Shi, Adsorption recovery of thorium(IV) by *Myrica rubra* tannin and larch tannin immobilized onto collagen fibres, *J. Radioanal. Nucl. Chem.* 260 (2004) 619–625.
- [25] Y.Y. Shen, R.L. Yang, Y. Liao, J. Ma, H. Mao, S.L. Zhao, Tannin modified aminated silica as effective absorbents for removal of light rare earth ions in aqueous solution, *Desalin. Water Treat.* (2015), doi: 10.1080/19443994.2015.1088479.
- [26] A. Mehdi, H. Alireza, K. Amir, Biosorption of lanthanum and cerium from aqueous solutions by grapefruit peel: Equilibrium, kinetic and thermodynamic studies meisam torab-mostaedi, *Res. Chem. Intermed.* 41 (2015) 559–573.
- [27] S.C. Tsai, T.H. Wang, Y.Y. Wei, W.C. Yeh, Y.L. Jan, S.P. Teng, Kinetics of Cs adsorption/desorption on granite by a pseudo-first-order reaction model, *J. Radioanal. Nucl. Chem.* 275 (2008) 555–562.
- [28] Y. Khambhaty, K. Mody, S. Basha, B. Jha, Biosorption of Cr(VI) onto marine *aspergillus niger*: Experimental studies and pseudo-second-order kinetics, *World J. Microbiol. Biotechnol.* 25 (2009) 1413–1421.
- [29] J.C. Moreno-Piraján, V.S. Garcia-Cuello, The removal and kinetic study of Mn, Fe, Ni and Cu ions from wastewater onto activated carbon from coconut shells, *Adsorption* 17 (2011) 505–514.
- [30] C.W. Cheung, J.F. Porter, G. McKay, Sorption kinetic analysis for the removal of cadmium ions from effluents using bone char, *Water Res.* 35 (2001) 605–612.